REPORT

TOPOLOGICAL MATTER

Distinguishing between non-abelian topological orders in a quantum Hall system

Bivas Dutta, Wenmin Yang, Ron Melcer, Hemanta Kumar Kundu, Moty Heiblum*, Vladimir Umansky, Yuval Oreg, Ady Stern, David Mross

Quantum Hall states can harbor exotic quantum phases. The nature of these states is reflected in the gapless edge modes owing to "bulk-edge" correspondence. The most studied putative non-abelian state is the spin-polarized filling factor (ν) = 5/2, which permits different topological orders that can be abelian or non-abelian. We developed a method that interfaces the studied quantum state with another state and used it to identify the topological order of ν = 5/2 state. The interface between two half-planes, one hosting the ν = 5/2 state and the other an integer ν = 3 state, supports a fractional ν = 1/2 charge mode and a neutral Majorana mode. The counterpropagating chirality of the Majorana mode, probed by measuring partition noise, is consistent with the particle-hole Pfaffian (PH-Pf) topological order and rules out the anti-Pfaffian order.

The quantum Hall effect (QHE) state harbors an insulating bulk and conductive edges and is the earliest known example of a topological insulator (*1*). It is characterized by topological invariants, which are stable to small changes in the details of the system (*2*). Of these quantities, the easiest to probe is the electrical Hall conductance of the edge mode, $G_H = \nu e^2/h$, where ν is the bulk filling factor (integer or fractional), e is the electron charge, and h is Planck's constant. Quantum Hall (QH) states with fractional filling factors support quasiparticles with fractional charges and anyonic statistics. The ubiquitous Laughlin states are abelian; exchanging the positions of their quasiparticles adds a phase to the ground-state wave function (*3*–*5*). In the more exotic non-abelian states (*6*, *7*), the presence of certain quasiparticles results in multiple degenerate ground states, and interchanging these quasiparticles cycles the system between the different ground states. In general, QH states permit different topological orders, and the usual conductance and charge measurements are not sufficient to distinguish between the different topological orders.

Another topological invariant, the thermal QH conductance G_T, may help make that distinction. The thermal conductance is sensitive to all energy-carrying edge modes, charged or neutral, and can be expressed as $G_T = KT$, where K is the thermal conductance coefficient and T is the temperature. It was proposed (*7*, *8*) and experimentally proven that K of a single chiral and ballistic mode—fermionic (*9*), bosonic (*10*, *11*), or (abelian) anyonic (*12*)—is quantized $K = \kappa_0$, with $\kappa_0 = \pi^2 k_B^2/3h$, where k_B is the Boltzmann constant. However, a fractional value of K is expected for non-abelian states (*13*). For the ν = 5/2 state, we found a thermal Hall conductance coefficient, $K = 2.5\kappa_0$, that is consistent with the non-abelian particle-hole Pfaffian (PH-Pf) topological order (*14*).

However, there is a caveat: For a QH state that supports multiple edge modes, some moving downstream (DS; in the chirality dictated by the magnetic field) and some upstream (US; in opposite chirality), the theoretically predicted thermal conductance assumes a full thermal equilibration among all modes (*15*–*17*). For example, for modes of integer thermal conductance, the predicted value is $G_T = (n_d - n_u)\kappa_0 T$, where n_d and n_u are the number of DS and US modes, respectively. In the other extreme, with no thermal equilibration, $G_T = (n_d + n_u)\kappa_0 T$ (*12*). Therefore, the thermal equilibration length, which is in general longer than the charge equilibration length, is of crucial importance in interpreting thermal conductance measurements.

Moore and Read predicted that the topological order of the ν = 5/2 state is a Pfaffian (Pf) state, with $K = 3.5\kappa_0$ (*18*). However, the Pf mode was ruled out when a US neutral mode was observed experimentally (*19*) because the Pf order does not support a topologically protected US mode. The "particle-hole conjugate" of the Pf order, the anti-Pfaffian (A-Pf) with $K = 1.5\kappa_0$ (*20*, *21*), does exhibit a US mode. Numerical studies found both Pf and A-Pf to be highly competitive ground states in a homogenous system (neglecting disorder). The two are degenerate within a single Landau level, and Landau level mixing may tip the balance between the two in either direction (*22*, *23*). Several theoretical proposals offer possible explanations for the discrepancy between numerical calculations and the experimentally found PH-Pf order: (i) Inhomogeneity in the density may lead to islands of local Pf and A-Pf orders, from which a global PH-Pf order emerges (*24*–*28*). (ii) A considerably longer thermal equilibration length than the size of the device may lead to deviation from the expected theoretical value. In particular, an unequilibrated Majorana mode in the A-Pf (*15*, *29*) order will add its contribution to K instead of subtracting it, leading to $K = 2.5\kappa_0$ (*30*–*32*).

One may suggest to measure the thermal conductance at a short propagation length, where thermal equilibration is practically negligible, expecting $K = (n_d + n_u)\kappa_0$; namely, $K_{A\text{-}Pf} = 4.5\kappa_0$ or $K_{PH\text{-}Pf} = 3.5\kappa_0$. However, "spontaneous edge reconstruction" may add short-lived pairs of counterpropagating (non-topological) neutral modes (*33*), thus increasing the apparent thermal conductance of the states at short distances.

We developed a method in which a studied state is interfaced with another state, with the interface harboring an isolated edge channel. We used this method to probe the Majorana modes' chirality at interfaces between the ν = 5/2 state and ν = 2 and ν = 3 integer states. Measurements fulfill two important requirements: (i) thermally unequilibrated transport, in which measurements are performed in the intermediate length regime—longer than the charge equilibration length (leading to the quantized interface conductance) but shorter than the thermal equilibration length (allowing unequilibrated modes transport) (*15*, *29*, *34*)—and (ii) compensating integer modes, in which the counterpropagating integer modes at the interface between ν = 5/2 and ν = 2 or 3 mutually localize each other. This eliminates spurious hotspots and allows the identification of the topological order.

We used gated high-quality GaAs-AlGaAs molecular beam epitaxy (MBE)–grown heterostructures (*35*). Structures were designed to resolve the contradictory requirements of the doped layers, which should ensure a full quantization of the fragile ν = 5/2 state and, at the same time, allow highly stable and "hysteresis-free" operation of the gated structures (*14*). Two separate gates divided the surface into two, an upper half and lower half (Fig. 1A). The gates were isolated from the sample and from each other by 15- to 25-nm layers of HfO_2 [more details of the structure are provided in (*35*)]. A gate-voltage in the range of $-1.5\ V < V_g < +0.3\ V$ allows varying the electron density from pinch off to $3 \times 10^{11}\ cm^{-2}$ (fig. S1). Tuning each gate separately controls the two interfaced filling factors, leading to the desired interface modes' conductance. The ohmic contacts at the physical edge of the mesa probe the filling

Braun Center for Sub-Micron Research, Department of Condensed Matter Physics, Weizmann Institute of Science, Rehovot 76100, Israel.
*Corresponding author. Email: moty.heiblum@weizmann.ac.il

factors of the two respective half-planes, and the contacts at the interface probe the interface.

The heart of the measurement setup (Fig. 1A, dashed box) consists of three ohmic contacts at the interface, with the source (Fig. 1A, "S"), placed symmetrically between the amplifier contact (Fig. 1A, "A") and the cold-grounded drain (Fig. 1A, "D"). An injected dc source current at the interface, I_S, forms a hotspot at the back side of the source (and at the front side of the drain) (*36*). In states that support counterpropagating modes, the thermally activated modes by the hotspot (usually, neutral modes), lead to shot noise at the amplifier contact (*37*, *38*). The noise was filtered with an LC resonance circuit, with a center frequency f_0 ~ 630 kHz and bandwidth Δf = 10 to 30 kHz, then amplified with a cold amplifier (cooled to 4.2 K) and a room-temperature amplifier, to be measured with a spectrum analyzer. Measurements were conducted at three different electron temperatures—10, 21, and 28 mK—and at different propagation lengths (between source and aplifier contacts): 28, 38, 48, and 58 μm.

The general strategy of the measurement is to place the lower-gated half-plane at the tested filling factor ν_{LG}, whereas the upper half-plane is always tuned to an integer filling, ν_{UG} = 0, 1, 2, 3. The defined chirality of the resultant interface edge modes is always with respect to the chirality of the tested state. For example, for $\nu_{LG} > \nu_{UG}$ the interface charge chirality is DS, whereas for $\nu_{LG} < \nu_{UG}$, the interface charge chirality is US. This is clearly noted in Figs. 1 to 3 (*35*). A description in terms of one-dimensional (1D) edge channels is a simplification, but one that is useful for illustrations and justified by the topological nature of the relevant phases. To measure the noise excited by the hotspot (at the back of the source) by a single amplifier, the magnetic

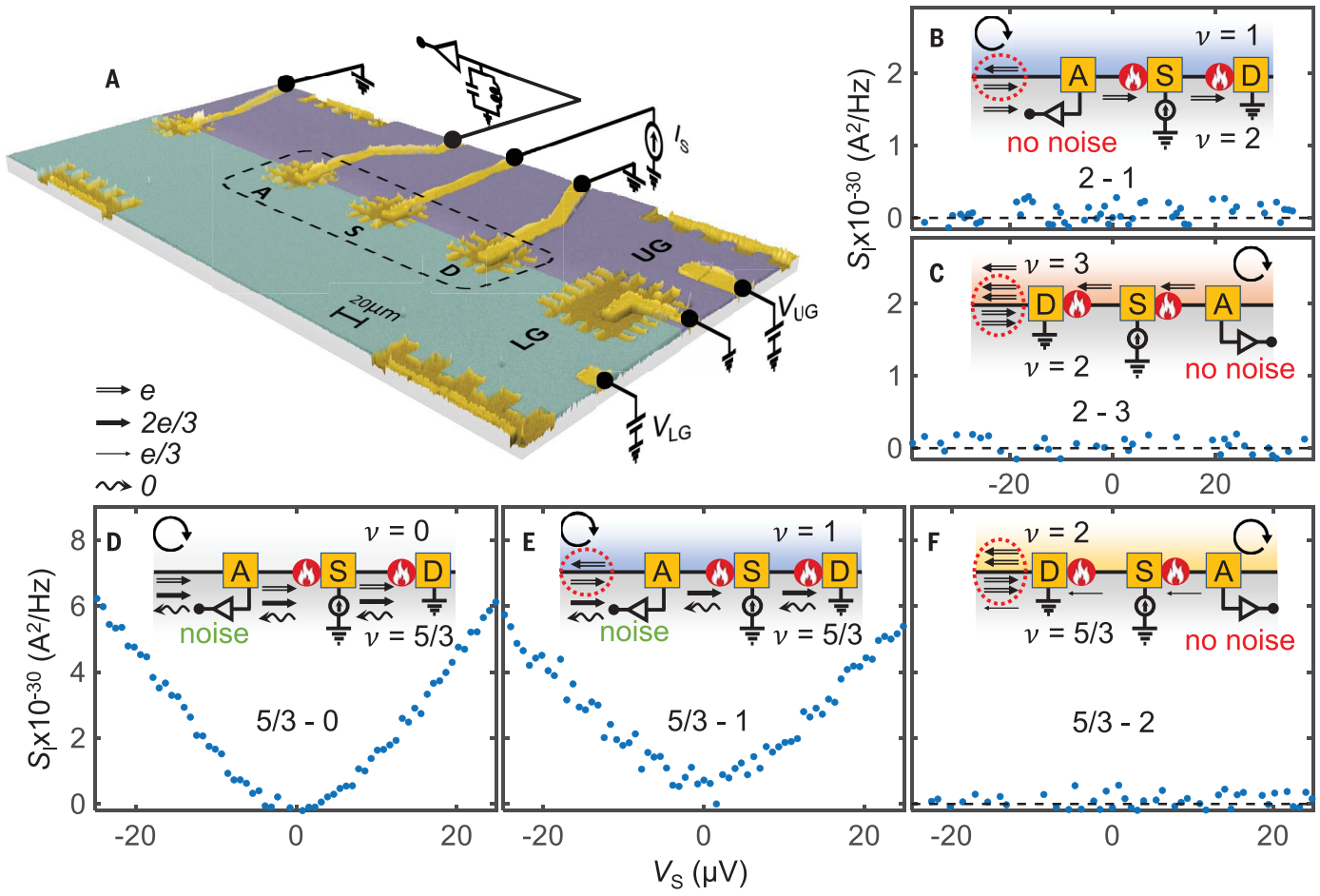

Fig. 1. Experimental setup to create and probe the interface between different states. (**A**) False-colors scanning electron microscopy image of a typical device. Ohmic contacts are in yellow, lower gte (LG) is light blue, and upper gate (UG) is purple. The two-dimensional electron gas (2DEG) is buried 200 nm below the surface [a detailed structure is available in (*35*)]. Gate voltages, V_{LG} and V_{UG}, control the density. The interface between the two planes hosts interface modes. Ohmic contacts at the edge probe the bulks' filling-factor. Ohmic contacts at the interface probe the interface modes. The heart of the device, highlighted by the dashed box, contains the source contact, S, placed at the same distance from the amplifier contact, A, and the drain contact, D, at different distances *S–A*: *L* = 28, 38, 48, and 58 μm. "Blocking contacts" avoid noise arriving at A from secondary hotspots (say, in the drain). (**B** and **C**) Interfaces of integer states ν = 2 with ν = 1 and ν = 3 at 10 mK. Counterpropagating integer modes at the interface are compensated, leaving a single integer mode at the interface, DS at the 2-1 interface, and US for the 2-3 interface. Hotspots (indicated with "red fire" symbols) are shown on the US side (2-1) and the DS side (2-3) of the source. Noise is not expected. (**D** to **F**) Interfacing the ν = 5/3 state at 10 mK. Arrows indicate four different types of edge modes: Double-line arrow indicates an integer-mode, thick-single arrow indicates a 2/3 charge mode, thin-single arrow indicates a 1/3 charge mode, and waved-arrow indicates a neutral mode. The incomplete circle with an arrowhead indicates the chirality. In (B) to (F), the schematic representation shows nonequilibrated to equilibrated modes from left to right. The 5/3-0 and the 5/3-1 interfaces are presented in the particle-like picture: DS integer 1 and 2/3 modes and US neutral mode. The 5/3-2 is presented in a hole-like picture: two DS integers 1 modes and a US 1/3 mode. The US neutral mode leads to noise in (D) and (E). In (F), a single US 1/3 mode remains, without any observed noise.

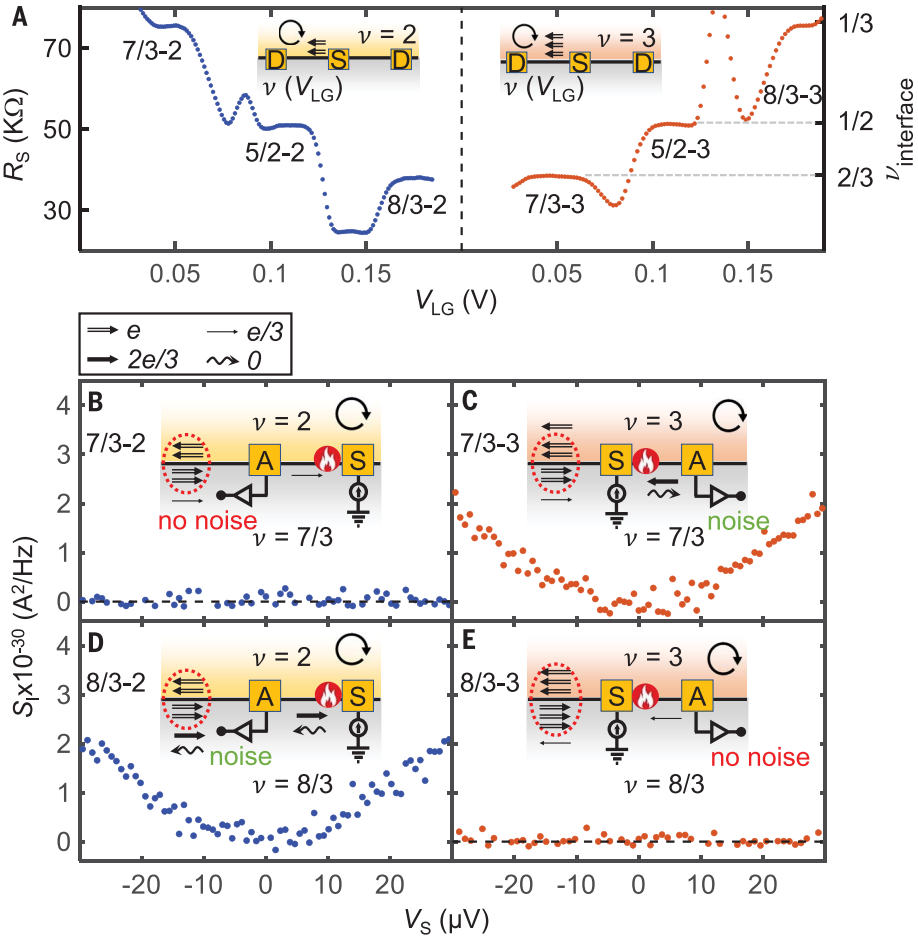

Fig. 2. Interfacing abelian fractional states in second Landau level. (**A**) Two-terminal resistance measured at the interface between ν = 2 (or 3) and ν = 7/3, 5/2, and 8/3. (Left) Upper plane is fixed at ν = 2 and (right) upper plane is fixed at ν = 3, whereas the lower plane is swept from ν = 7/3 to ν = 8/3. Clear quantized plateaus corresponding to (left) ν = 1/3, 1/2, and 2/3 and (right) ν = 2/3, 1/2, and 1/3, accurate to ~1%, are observed. Peaks and valleys in between plateaus are caused by reentrant filling factors. (**B**) Interface between ν = 7/3 and ν = 2 at 21 mK. The two integer modes are compensated, leaving the DS 1/3 charge mode. No noise is observed. (**C**) Interface between ν = 7/3 and ν = 3 at 21 mK. Two integer modes are compensated, leaving one US integer and a downstream 1/3. The equilibration of these two counterpropagating charge modes gives rise to an upstream ν = 2/3 charge mode and a downstream neutral mode, accompanied by noise. (**D**) Interface between ν = 8/3 and ν = 2 at 21 mK. Two integer modes are compensated, leaving a DS ν = 2/3 charge mode accompanied by a US neutral mode. US noise is observed. (**E**) Interface between ν = 8/3 and ν = 3 at 21 mK. The equilibration between the integers at the interface leaves a single US charge mode ν = 1/3, with no noise. The arrows in the top left box of (B) to (E) indicate bosonic edge modes with the indicated two-terminal electric conductance.

field was reversed (and therefore, so was the chirality) under these two interfacing conditions. In Figs. 1 to 3, for convenience, we flip the amplifier's position instead of the chirality (for example, Fig. 1, B and C).

In Fig. 1, B and C, we show a relatively simple experimental test of interfacing the integer ν = 2 state (tested state) with ν = 1 and ν = 3. The injected DC current, I_S, leads to a hotspot at the US side of the source in Fig. 1B and at the DS side of the source in Fig. 1C, respectively. A perfect charge equilibration took place for all four lengths and three temperatures, with two terminal interface resistance (R_S) = h/e^2; there was no observed US (Fig. 1B) or DS (Fig. 1C) noise. This suggests that the presence of any residual nonequilibrated current (which may persist in spite of charge equilibration) does not lead to observable noise.

Before testing interfacing in the second Landau level, we tested the "interfacing method" with a more complex abelian state in the first Landau level, which involves counterpropagating modes (charge and neutral). We interfaced the ν = 5/3 = 1 + 2/3 filling with the integers ν = 0, 1, 2. We used two similar descriptions of this configuration (fig. S4). The first assumes that the two half-planes are initially separated, and each of them supports its own edge modes (Fig. 1, E and F). With an intimate proximity at the interface, the integer modes on both sides of the interface compensate each other, leaving only fractional interface modes. In the case of 5/3 interfaces, the integer modes of ν = 1 or ν = 2 are localized, with propagating interface DS ν = 2/3 (with neutral) or US ν = 1/3 modes, respectively (fig. S4, E and G). The second approach is to regard the integer filling ν_{UG} at the upper half-plane as a "vacuum" on which a filling $\nu_{LG} - \nu_{UG}$ resides in the lower half-plane. Consequently, the common ν_{UG} integer modes circulate around the periphery of the mesa, and the interface carries an edge structure of filling $\nu_{LG} - \nu_{UG}$ (fig. S4, F and H). We mostly used the first approach.

We returned to the present test of interfacing the 5/3 state (Fig. 1, D to F). Interfacing 5/3-0 or 5/3-1 supports an integer and a fractional ν = 2/3 charge modes or a fractional ν = 2/3 charge mode, respectively, accompanied by an excited US bosonic neutral mode (*39*–*41*), leading to the observed US noise (Fig. 1, D and E). Alternatively, interfacing 5/3-2, the compensated integer modes leave behind a single US ν = 1/3 mode at the interface, with no noise observed (Fig. 1F).

We next concentrated on interfacing the dominant fractional states in the second Landau level, ν = 7/3, ν = 5/2, and ν = 8/3 with the integers ν = 2 and ν = 3. Testing first charge equilibration, we fixed the integer filling in the upper half-plane and swept the density of the lower half-plane (Fig. 2A). Clear conductance plateaus, accurate to about 1% (with reentrant peaks and valleys between plateaus), were observed at all propagation lengths and temperatures.

The interfaced 7/3-2 configuration compensates the two integer modes, leaving a DS edge mode of ν = 1/3, with no US noise (Fig. 2B; the chirality is indicated in Fig. 2A). By contrast, the interfaced 7/3-3 configuration leaves the familiar US ν = 2/3 charge mode and a DS bosonic neutral mode (Fig. 2C). The hotspot at the source excites the neutral mode with a DS noise at the amplifier. Interfacing ν = 8/3 with ν = 2 compensates the two integers and leaves a DS charge mode of ν = 2/3 and an US excited bosonic neutral mode (Fig. 2D). By contrast, interfacing the state with ν = 3 leaves

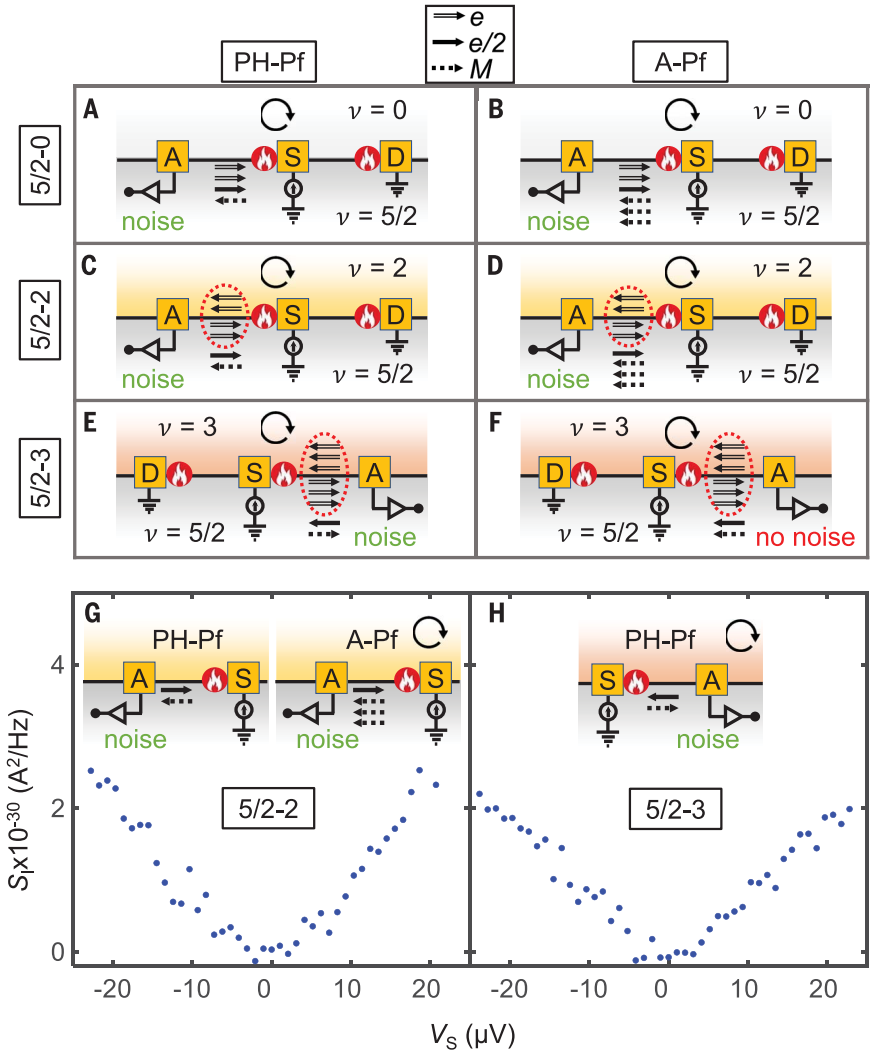

Fig. 3. Interfacing the ν = 5/2 states with ν = 2 and ν = 3. Comparison of edge structures for the PH-Pf and the A-Pf orders with ν = 0, 2, and 3. (**A** and **B**) Edge structure of ν = 5/2 state at the edge of sample presented in particle-like presentation. Because US noise is expected for both orders, this measurement cannot distinguish between the two orders. (**C** and **D**) Interfacing 5/2-2 for both topological orders. US noise is expected for both orders. (**E** and **F**) Interfacing 5/2-3 for both orders, presented for convenience, in the hole-like picture. The three integer modes at the interface are compensated, leaving at the interface PH-Pf, with a US 1/2 charge mode and a DS neutral Majorana mode, and A-Pf, with copropagating US 1/2 charge and neutral Majorana modes. DS noise is expected for the PH-Pf order, whereas no noise is expected for the A-Pf order. (**G**) Measured US noise at the interface of 5/2-2 at 10 mK, which is consistent with both of the competing orders. (**H**) Measured DS noise at the 5/2-3 interface at 10 mK, which is expected only for the PH-Pf order. Double-line arrow indicates an integer-mode, thick-single arrow indicates a 1/2-mode, and the dashed-arrow indicates a Majorana-mode. The incomplete circled arrow indicates the chirality.

a US ν = 1/3 charge mode at the interface, with no resulting noise (Fig. 2E).

Before presenting the main experimental results, it is worth discussing the outcome of interfacing the PH-Pf and A-Pf orders of ν = 5/2 with the integers ν = 0, 2, 3 (Fig. 3, A to F). The consequence of a similar interfacing of other proposed orders of ν = 5/2 are described in figs. S10 and S11 (*35*). The mode structure of the two topological orders of ν = 5/2 with vacuum—at the 5/2-0 interface—are shown in Fig. 3, A and B. For both orders, the 5/2-2 interface leaves a DS fractional charge mode ν = 1/2 and US Majorana modes, one for the PH-Pf and three for A-Pf orders (Fig. 3, C and D). The 5/2-3 interface is more interesting. An interface of the PH-Pf ν = 5/2 with ν = 3 supports counterpropagating US fractional charge mode ν =1/2 and a DS Majorana mode (Fig. 3E), whereas for the interface of the A-Pf ν = 5/2 and ν = 3, the latter two modes co-propagate in the US direction (Fig. 3F). Therefore, measuring the chirality of the Majorana mode at the 5/2-3 interface is crucial for identifying the actual topological order of the ν = 5/2 state.

The noise data for 5/2 interfaces are shown in Fig. 3, G and H, measured at 10 mK with a propagation length of 28 μm. Noise was found in the US direction at the interface 5/2-2 (no noise observed in DS) and in the DS direction for 5/2-3 (no US noise was observed), both with similar amplitude at the same source voltage. As discussed above, the measured DS noise at the 5/2-3 interface points at the existence of the PH-Pf order (Fig. 3H, inset). Measurements at all temperatures and lengths (with two different MBE growths and two thermal cycles) led to similar results (figs. S33 and S34). This is the main result of our work.

The PH-Pf is a particle-hole symmetric state. Therefore, the same outcome should occur when it is interfaced with ν = 2, where the system is regarded as a half-filled level of electrons on top of two full Landau levels, and with ν = 3, where the system is regarded as a half-filled Landau level of holes on top of three full Landau levels. Our results manifest this particle-hole symmetry.

The amplitude of the neutral noise as function of the number of compensated integer modes is also important. Given that the temperature of the hotspot (T_{HS}) is proportional to the applied voltage ($T_{HS}^2 \sim KV_S^2$), we plotted the noise data as a function of the source voltage at a fixed propagation length of 28 μm, for a few interfacing conditions (Fig. 4A). The noise (US or DS) was similar for all integers *n*. The same behavior was also observed for the 8/3-*n* interfaces (fig. S17B). These results indicate that the integers' hotspots, located at the boundary of the large source ohmic contact, do not take part in the excitation of the neutral (bosonic or Majorana) modes. The latter are excited by the hotspot generated by interedge equilibrations, which are somewhat remote from the source contact (*15*, *29*). The dependence of the noise on the propagation length, for the 5/2-*n* and 8/3-*n* interfaces, is shown in Fig. 4B (the solid lines are guides to the eye), indicating a qualitatively similar thermal equilibration process of the "different neutrals" as the propagation length is increased. In fig. S24, we add similar measurements of the interfaces 5/3-*n* and 2/3-0.

The measured results are naturally explained in terms of interfaces between a PH-Pf topological order of ν = 5/2 and the integers ν = 2 and ν = 3. However, we cannot exclude the possibility of edge reconstruction that might give rise to noise at the interface. In particular, this may include a scenario in which the presence of an interface to an integer filling makes

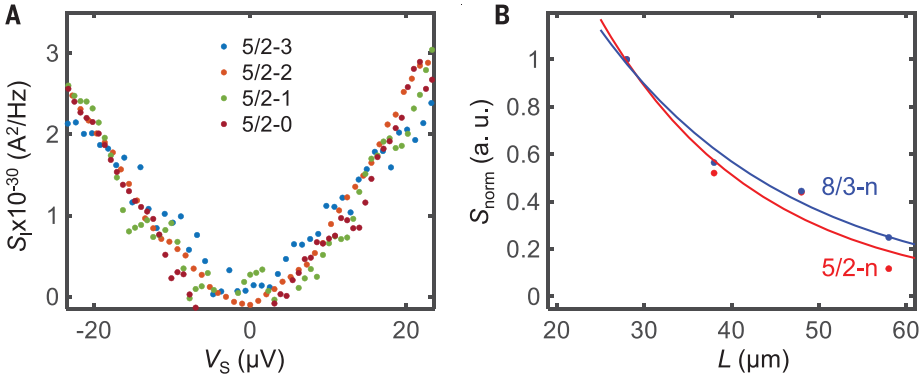

Fig. 4. Dependence of the noise owing to neutral modes on the number of integer modes and the propagation length. (**A**) Noise in a few interfacing conditions, 5/2-*n* with *n* = 0, 1, 2, and 3, measured at 10 mK and for 28 μm propagation length. The measured US noise (and DS noise for 5/2-3) is independent of *n*, indicating that the integer modes do not play a role in the excitation of the neutral modes. A similar observation is found also for 8/3-*n*, with *n* = 0, 1, and 2 (fig. S17B). (**B**) The measured noise as a function of distance (normalized to the noise at 28 μm). The solid lines are guides to the eye. Because the noise amplitude does not depend on the number of integer modes [as seen in (A)], the data for ν = 5/2 and ν = 8/3 are annotated as 5/2-*n* and 8/3-*n*. The noise decay length is qualitatively similar for both 5/2-*n* and 8/3-*n*.

the topological order of the ν = 5/2 close to the interface different from that of the bulk. A specific example of an interface reconstruction in the A-Pf bulk is discussed in (*35*). However, there is no indication for such edge reconstruction in the whole set of the measurements we performed on interfaces of the abelian cases. A thermal metal (*25*–*28*) at nonzero temperatures may exhibit similar edge physics as that of PH-Pf (*27*) while having small but nonzero bulk longitudinal thermal conductance. This scenario cannot be ruled out by these measurements.

In this work, we have introduced a method that is instrumental in identifying the topological order of the non-abelian ν = 5/2 state. Because the previous experimental determination of the PH-Pf order was based on full thermal equilibration of all modes (*12*, *14*), questions were raised as to whether this condition was fulfilled (*15*, *30*). Here, by forming chiral 1D modes at the interface between two half-planes, each with a different filling factor, leading to a single ν = 1/2 charge mode and Majorana modes, we considerably strengthen the case for a PH-Pf topological order of the ν = 5/2 state and weaken that of its competitors (*6*, *35*, *42*–*44*).

In a broader perspective, a similar interfacing method between quantum states can be used to engineer distinct fractional 1D interface modes, which do not live on the physical edge of the sample. Our method may enable the study of the rich world of non-abelian quasiparticles, including as yet unexplored states such as the theoretically proposed non-abelian ν = 12/5 state.

REFERENCES AND NOTES

1. B. I. Halperin, J. K. Jain, *Fractional Quantum Hall Effects: New Developments*. B. I. Halperin, J. K. Jain, Eds. (World Scientific, 2020).
2. X.-G. Wen, *Quantum Field Theory of Many-Body Systems: From the Origin of Sound to an Origin of Light and Electrons* (Oxford Univ. Press, 2004).
3. B. I. Halperin, *Phys. Rev. Lett.* **52**, 1583–1586 (1984).
4. D. Arovas, J. R. Schrieffer, F. Wilczek, *Phys. Rev. Lett.* **53**, 722–723 (1984).
5. J. M. Leinaas, J. Myrheim, *Nuovo Cimento B* **37**, 1–23 (1977).
6. X. G. Wen, *Phys. Rev. Lett.* **66**, 802–805 (1991).
7. J. B. Pendry, *J. Phys. Math. Gen.* **16**, 2161–2171 (1983).
8. C. L. Kane, M. P. A. Fisher, *Phys. Rev. B Condens. Matter* **55**, 15832–15837 (1997).
9. S. Jezouin *et al.*, *Science* **342**, 601–604 (2013).
10. K. Schwab, E. A. Henriksen, J. M. Worlock, M. L. Roukes, *Nature* **404**, 974–977 (2000).
11. M. Meschke, W. Guichard, J. P. Pekola, *Nature* **444**, 187–190 (2006).
12. M. Banerjee *et al.*, *Nature* **545**, 75–79 (2017).
13. N. Read, D. Green, *Phys. Rev. B Condens. Matter* **61**, 10267–10297 (2000).
14. M. Banerjee *et al.*, *Nature* **559**, 205–210 (2018).
15. K. K. W. Ma, D. E. Feldman, *Phys. Rev. B* **99**, 085309 (2019).
16. K. K. W. Ma, D. E. Feldman, *Phys. Rev. Lett.* **125**, 016801 (2020).
17. A. Aharon-Steinberg, Y. Oreg, A. Stern, *Phys. Rev. B* **99**, 041302 (2019).
18. G. Moore, N. Read, *Nucl. Phys. B* **360**, 362–396 (1991).
19. A. Bid *et al.*, *Nature* **466**, 585–590 (2010).
20. M. Levin, B. I. Halperin, B. Rosenow, *Phys. Rev. Lett.* **99**, 236806 (2007).
21. S. S. Lee, S. Ryu, C. Nayak, M. P. Fisher, *Phys. Rev. Lett.* **99**, 236807 (2007).
22. M. P. Zaletel, R. S. K. Mong, F. Pollmann, E. H. Rezayi, *Phys. Rev. B Condens. Matter Mater. Phys.* **91**, 045115 (2015).
23. E. H. Rezayi, *Phys. Rev. Lett.* **119**, 026801 (2017).
24. P. T. Zucker, D. E. Feldman, *Phys. Rev. Lett.* **117**, 096802 (2016).
25. D. F. Mross, Y. Oreg, A. Stern, G. Margalit, M. Heiblum, *Phys. Rev. Lett.* **121**, 026801 (2018).
26. C. Wang, A. Vishwanath, B. I. Halperin, *Phys. Rev. B* **98**, 045112 (2018).
27. I. C. Fulga, Y. Oreg, A. D. Mirlin, A. Stern, D. F. Mross, *Phys. Rev. Lett.* **125**, 236802 (2020).
28. B. Lian, J. Wang, *Phys. Rev. B* **97**, 165124 (2018).
29. J. Park, C. Spånslätt, Y. Gefen, A. D. Mirlin, *Phys. Rev. Lett.* **125**, 157702 (2020).
30. S. H. Simon, B. Rosenow, *Phys. Rev. Lett.* **124**, 126801 (2020).
31. S. H. Simon, *Phys. Rev. B* **97**, 121406 (2018).
32. D. E. Feldman, *Phys. Rev. B* **98**, 167401 (2018).
33. R. Bhattacharyya, M. Banerjee, M. Heiblum, D. Mahalu, V. Umansky, *Phys. Rev. Lett.* **122**, 246801 (2019).
34. S. K. Srivastav *et al.*, *Phys. Rev. Lett.* **126**, 216803 (2021).
35. Materials and methods are available as supplementary materials.
36. U. Klaß, W. Dietsche, K. Vonklitzing, K. Ploog, *Z. Phys. B Condens. Matter* **82**, 351–354 (1991).
37. J. Park, A. D. Mirlin, B. Rosenow, Y. Gefen, *Phys. Rev. B* **99**, 161302 (2019).
38. C. Spånslätt, J. Park, Y. Gefen, A. D. Mirlin, *Phys. Rev. Lett.* **123**, 137701 (2019).
39. C. L. Kane, M. P. Fisher, J. Polchinski, *Phys. Rev. Lett.* **72**, 4129–4132 (1994).
40. J. Wang, Y. Meir, Y. Gefen, *Phys. Rev. Lett.* **111**, 246803 (2013).
41. Y. Meir, *Phys. Rev. Lett.* **72**, 2624–2627 (1994).
42. G. Yang, D. E. Feldman, *Phys. Rev. B Condens. Matter Mater. Phys.* **90**, 161306 (2014).
43. B. Overbosch, X.-G. Wen, Phase transitions on the edge of the ν = 5/2 Pfaffian and anti-Pfaffian quantum Hall state. arXiv:0804.2087 [cond-mat.mes-hall] (2008).
44. B. I. Halperin, *Helv. Phys. Acta* **56**, 75–102 (1983).
45. B. Dutta *et al.*, Data for: Distinguishing between non-abelian topological orders in a quantum Hall system, Zenodo (2021); doi: 10.5281/zenodo.5638894.

ACKNOWLEDGMENTS

We acknowledge valuable discussions with B. Halperin, M. Banerjee, and N. Schiller. B.D. acknowledges D. Mahalu for her help with E-beam lithography. **Funding:** B.D. acknowledges the support from Clore Foundation. M.H. acknowledges the continuous support of the Sub-Micron Center staff, the support of the European Research Council under the European Community's Seventh Framework Program (FP7/2007-2013)/ERC under grant agreement 713351, the partial support of the Minerva foundation under grant 713534, and together with V.U. the German Israeli Foundation (GIF) under grant I-1241-303.10/2014. D.M. acknowledges support from the ISF (1866/17) and the CRC/Transregio 183. Y.O. and A.S. acknowledge partial support through the ERC under the European Union's Horizon 2020 research and innovation program (grant agreement LEGOTOP 788715), the ISF Quantum Science and Technology (2074/19), and the CRC/Transregio 183. Y.O. acknowledges support from the BSF and NSF (2018643). **Author contributions:** B.D. and W.Y. designed and fabricated the devices. W.Y. participated in the initial measurements and fabrications. B.D. performed the measurements, with help of W.Y. in the initial part and H.K.K. in the later part. B.D., H.K.K., and R.M. participated in understanding the data, with guidance throughout from M.H. Y.O., A.S., and D.M. worked on the theoretical aspects. V.U. developed and grew the heterostructures supporting the 2DEG. **Competing interests:** The authors declare no competing interests. **Data and materials availability:** All the data presented in this paper are publicly available at Zenodo (*45*).

SUPPLEMENTARY MATERIALS

science.org/doi/10.1126/science.abg6116
Materials and Methods
Supplementary Text
Figs. S1 to S34
Tables S1 and S2
References (*46*–*51*)

17 January 2021; accepted 16 November 2021
10.1126/science.abg6116